Symmetry Breaking Dynamics in Quantum Many-Body Systems

Hui Yu[1], Zi-Xiang Li[1,2*], and Shi-Xin Zhang[1*]

[1]*Beijing National Laboratory for Condensed Matter Physics and Institute of Physics, Chinese Academy of Sciences, Beijing 100910, China*
[2]*University of Chinese Academy of Sciences, Beijing 100049, China*

(Received 14 August 2025; accepted manuscript online 11 September 2025)

Entanglement asymmetry (EA) has emerged as a powerful tool for characterizing symmetry breaking in quantum many-body systems. In this Letter, we explore how symmetry is dynamically broken through the lens of EA in two distinct scenarios: a non-symmetric Hamiltonian quench and a non-symmetric random quantum circuit, with a particular focus on U(1) symmetry. In the former case, symmetry remains broken in the subsystem at late times, whereas in the latter case, the symmetry is initially broken and subsequently restored, consistent with the principles of quantum thermalization. Notably, the growth of EA exhibits unexpected overshooting behavior at early times in both contexts, contrasting with the behavior of charge variance. We also consider dynamics of non-symmetric initial states under the symmetry-breaking evolution. Due to the competition of symmetry-breaking in both the initial state and Hamiltonian, the early-time EA can increase and decrease, while quantum Mpemba effects remain evident despite the weak symmetry-breaking in both settings.

DOI: 10.1088/0256-307X/42/11/110602 CSTR: 32039.14.0256-307X.42.11.110602

1. Introduction. Symmetry breaking is a ubiquitous phenomenon across all branches of physics. A well-known example is the Higgs mechanism[1] in particle physics, where the vacuum state of the universe causes different particles to acquire mass, spontaneously breaking the electroweak symmetry. This type of symmetry breaking, which occurs without external influences, is referred to as spontaneous symmetry breaking (SSB). In contrast, a symmetry can also be explicitly broken when the Hamiltonian describing the system directly breaks the symmetry. How symmetry breaks dynamically in this case is an interesting fundamental question to explore.

Symmetry properties are also closely related to the concept of quantum thermalization[2–6] for generic quantum many-body systems. In general, when a closed quantum system evolves with a chaotic Hamiltonian, the reduced density matrix of a small subsystem a thermalizes to the equilibrium finite-temperature state: $\rho_a \propto \exp(-\beta \hat{H}_a)$ where $\hat{H}_a$ is the Hamiltonian of the subsystem and β is a Lagrangian multiplier determined by the initial energy density. Symmetry is restored at later times for symmetric Hamiltonian $\hat{H}_a$, since $[\hat{Q}_a, \rho_a] = 0$ where $\hat{Q}_a$ represents the corresponding symmetry generator. However, if $\hat{H}_a$ does not respect the symmetry, the reduced density matrix ρ_a at late times is non-commuting with $\hat{Q}_a$. In this case, symmetry breaking persists even if the system begins in a symmetric state. It is important to distinguish this explicit breaking from SSB. In the thermodynamic limit, SSB enables a low-temperature symmetric initial state to evolve dynamically into a symmetry-broken steady state. In contrast, for finite-size systems, SSB cannot occur, and the equilibrium state must retain the symmetry of the Hamiltonian.

Apart from the richness of the late-time behavior, early-time dynamics have also garnered significant attention. For example, the Mpemba effect,[7] which claims that hot water freezes faster than cold water, has been widely explored in both classical and quantum contexts.[8–23] Recently, quantum Mpemba effect (QME) was reported in integrable systems and chaotic systems.[24–26] QME refers to the phenomenon where, during relaxation toward a steady state value, the time evolution curves of a physical quantity for different initial conditions cross each other. For instance, U(1)-symmetry restoration occurs more rapidly for more asymmetric initial states under the U(1)-symmetric Hamiltonian quench.[27–37] This finding was subsequently explored in various other settings[38–47] and experimentally realized on a trapped-ion quantum simulator.[48]

Previous studies[24,25] have primarily focused on characterizing symmetry restoration when an asymmetric initial state evolves under a symmetric Hamiltonian or random circuit. In contrast, this Letter examines the dynamical aspects of symmetry breaking, exploring the behavior of symmetric and asymmetric initial states under non-symmetric evolution.[49] In addition, due to experimental limitations, symmetric evolutions are often affected by noise and defects, resulting in non-symmetric contributions as well. In such cases, can symmetry restoration still occur, or does symmetry breaking become more pronounced over time? Additionally, how does QME behave in the presence of symmetry-breaking interactions? Addressing these questions offers a more comprehensive understanding of symmetry and symmetry breaking in quantum many-body systems.

*Corresponding authors. Email: zixiangli@iphy.ac.cn; shixinzhang@iphy.ac.cn

In this Letter, we investigate and compare the dynamics of symmetry breaking with two distinct models: a non-symmetric random circuit [50] and a non-symmetric Hamiltonian evolution, each with different symmetric and asymmetric initial states. To characterize the extent of symmetry breaking in subsystem a, we employ the metric of entanglement asymmetry (EA),[24] which has been extensively utilized as a measure of symmetry breaking in quantum field theories [51–53] and out-of-equilibrium many-body systems.[39,41,54]. EA is defined as

$$\Delta S_a = S(\rho_{a,Q}) - S(\rho_a)\,. \tag{1}$$

Here, $S(\rho_a)$ denotes the standard Von Neumann entropy of subsystem a, and $\rho_{a,Q} = \sum_{q\in\mathbb{Z}} \Pi_q \rho_a \Pi_q$ where $\hat{Q}_a = \sum_{i\in a} \sigma_i^z$ in case of U(1) symmetry and Π_q is the projector onto eigenspace of $\hat{Q}_a$ with charge q. Consequently, $\rho_{a,Q}$ is block diagonal in the eigenbasis of $\hat{Q}_a$. The EA satisfies two key properties: (1) $\Delta S_a \geq 0$ since the EA is the relative entropy between $\rho_{a,Q}$ and ρ_a. (2) $\Delta S_a = 0$ if and only if $\rho_{a,Q} = \rho_a$. In random circuit settings, $\mathbb{E}[\Delta S_a]$ is employed as the circuit-averaged value of ΔS_a. Note that the symmetry for subsystem mixed states investigated here corresponds to the weak symmetry in Refs. [55,56]. In parallel with the analysis of EA, we also compute the charge variance (CV) $\sigma_Q^2 = \langle \hat{Q}^2\rangle - \langle \hat{Q}\rangle^2$, where $\hat{Q} = \sum_{i=1}^{L} \sigma_i^z$. This quantity serves as a measure of charge fluctuations within the system, offering a complementary perspective on symmetry breaking.

For a non-symmetric Hamiltonian evolution, we find that U(1) symmetry cannot be restored in a subsystem, which can be explained by the late-time reduced density matrix relaxing to the form $\exp(-\beta \hat{H}_a)$, where $\hat{H}_a$ explicitly includes symmetry-breaking terms. In this scenario, the EA shows nontrivial overshooting at early times, characterized by a peak in EA that significantly exceeds its late-time saturation value. This behavior contrasts with other symmetry-breaking measures like CV and mirrors the thermal overshooting of the classical Mpemba effect,[11] where systems transiently exceed their equilibrium temperature. Furthermore, the QME originating from symmetric evolution disappears when the strength of symmetry breaking in the evolution exceeds some thresholds.

In the case of non-symmetric random circuits, we show that U(1) symmetry for a small subsystem can still be restored regardless of the initial states. As a result, EA also exhibits overshooting at early times. Additionally, QME appears at early times, unless all U(1)-symmetric gates are replaced by random Haar gates, where EA dynamics are the same for different U(1)-asymmetric initial states.

2. Setup. To study dynamics in these systems, we consider three initial states: the ferromagnetic state $|000...0\rangle$, the antiferromagnetic state $|0101..1\rangle$, and the domain-wall state $|000..111\rangle$, where the domain wall is positioned at the center of the chain. To incorporate the effect of symmetry breaking in the initial state, we introduce tilted ferromagnetic states,[24,25] defined as

$$|\psi_i(\theta)\rangle = \exp\left(-\mathrm{i}\frac{\theta}{2}\sum_j \sigma_j^y\right)|000...0\rangle\,, \tag{2}$$

where σ_j^y is the Pauli-y matrix on the j-th qubit, and θ is a tuning parameter controlling the strength of symmetry breaking in the initial state. When $\theta = 0$, equation (2) is U(1)-symmetric with zero EA. As θ increases, the EA grows, reaching its maximum value at $\theta = \pi/2$. The tilted antiferromagnetic and tilted domain wall states are constructed in a similar manner.

The random circuit architecture consists of two-qubit U(1)-symmetric gates and Haar-random gates arranged in a brick-wall pattern. The U(1)-symmetric gates have a block-diagonal matrix structure, with each block independently sampled from the Haar measure.[57–59] The effect of symmetry breaking depends on the density (doping probability) of random Haar gates without U(1) symmetry, denoted as P_{Haar}. The time unit in the circuit is defined by the application of two consecutive layers of gates. $\mathbb{E}[\Delta S_a]$ is computed by averaging over 5000 circuit configurations.

We also investigate Hamiltonian dynamics where the state $|\psi_i(\theta)\rangle$ undergoes unitary evolution by $\exp(-\mathrm{i}Ht)|\psi_i(\theta)\rangle$, and the Hamiltonian is

$$\begin{aligned} H \;=\; & -\frac{1}{4}\sum_{j=1}^{L}\left(\sigma_j^x\sigma_{j+1}^x + \gamma\sigma_j^y\sigma_{j+1}^y + \Delta_1\sigma_j^z\sigma_{j+1}^z\right) \\ & - \Delta_2\sum_{j=1}^{L}\left(\sigma_j^x\sigma_{j+2}^x + \sigma_j^y\sigma_{j+2}^y + \sigma_j^z\sigma_{j+2}^z\right). \end{aligned} \tag{3}$$

Here, L denotes the total system size, while Δ_1 and Δ_2 represent the coefficients for nearest-neighbor and next-nearest-neighbor interactions, respectively. Δ_2 introduces non-integrability, and γ controls the strength of symmetry breaking. Periodic boundary conditions are imposed in both contexts.

3. U(1)-Symmetric Initial States with U(1) Non-Symmetric Hamiltonian. All numerical simulations are performed using the TensorCircuit-NG package.[60] Here, we investigate the dynamics of symmetry breaking under an integrable Hamiltonian H_1 with $\Delta_1 = 0.4$ and $\Delta_2 = 0$, and a non-integrable Hamiltonian H_2 with $\Delta_1 = 0.4$ and $\Delta_2 = 0.05$, with system size $L = 12$ sites. As revealed in Figs. 1(a) and 1(b), EA for various different Hamiltonian symmetry-breaking γ exhibits peaks at early times that are much larger than steady values. Furthermore, the peak value of the EA, $(\Delta S_{L/3})_{\max}$, is found to be correlated with the strength of symmetry breaking, $1-\gamma$, for different symmetric initial states as shown in Fig. 1(c), where EA of the ground state of H_1 follows the same trend. Notably, the peak heights nearly coincide between the ferromagnetic and domain wall states, as the early-time peak primarily depends on the local configurations of the initial state. Moreover, the finite-size scaling analysis demonstrates the existence of this peak in the thermodynamic limit [see the Supplementary Materials (SM)].

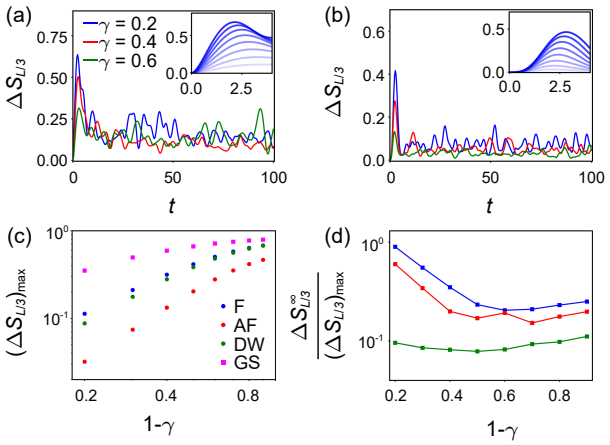

Fig. 1. EA as a function of time with (a) ferromagnetic and (b) antiferromagnetic states for different values of γ under H_1. The insets show the peak of EA at different values of γ. From bottom to top: $\gamma = 0.8, 0.7, 0.6, 0.5, 0.4, 0.3, 0.2, 0.1$. Panels (c) and (d) show the peak value of EA, $(\Delta S_{L/3})_{\max}$, and the ratio of the late-time EA, $\Delta S^{\infty}_{L/3}$, to $(\Delta S_{L/3})_{\max}$ as a function of $1-\gamma$ for various initial states under H_1. GS denotes the value of EA calculated from the ground state of H_1.

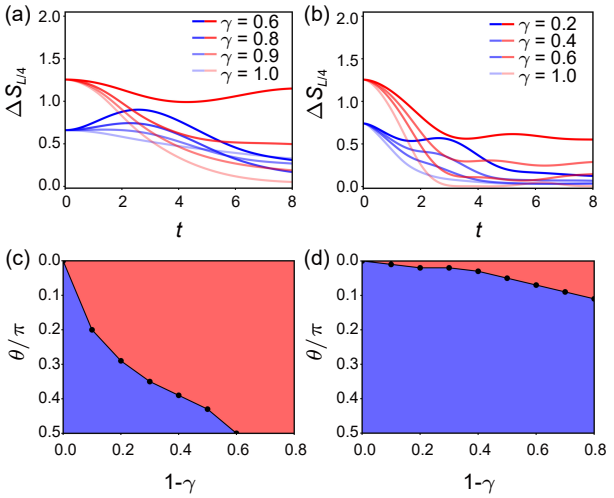

Fig. 2. EA dynamics for (a) tilted ferromagnetic states and (b) tilted antiferromagnetic states with varying γ. The blue curves correspond to $\theta = 0.2\pi$, and the red curves represent $\theta = 0.5\pi$. Panels (c) and (d) depict the dependence of early-time EA dynamics on θ and $1-\gamma$ for ferromagnetic and antiferromagnetic states, respectively. When the parameter is in the red region, EA can exceed the initial value, while in the blue region, EA firstly decreases and never grows higher than the initial value. All black dots are obtained through numerical simulation. All calculations are based on H_1.

By analyzing Fig. 1, we identify that the late-time EA $\Delta S^{\infty}_{L/3}$ oscillates and does not approach zero. This is because the reduced density matrix of subsystem a evolves towards a canonical ensemble $\exp(-\beta \hat{H}_a)$, where $\hat{H}_a$ has the same form as $\hat{H}$ in Eq. (3), but acts solely on subsystem a. Since $\hat{H}_a$ includes symmetry-breaking terms, $[\rho_a, \hat{Q}_a] \neq 0$, leading to a non-vanishing EA at long times. In Fig. 1(d), we calculate the ratio of $\Delta S^{\infty}_{L/3}$ to $(\Delta S_{L/3})_{\max}$ with varying γ. The late-time EA, $\Delta S^{\infty}_{L/3}$, is obtained by averaging $\Delta S_{L/3}$ over 2000 time points between $t_1 = 2000$ and $t_2 = 40000$. The results further confirm the overshooting behavior as the late-time saturating EA value is much lower than the early-time peak value. This phenomenon stems from the competition between symmetry breaking and subsystem decoherence. Initially, the non-symmetric Hamiltonian dynamically generates asymmetry, causing EA to grow as symmetry breaking predominates over decoherence. Later, symmetry breaking saturates while decoherence becomes the sole governing factor for EA evolution, driving EA toward a steady-state value. The early-time peak emerges from the intricate interplay between these competing effects. On the contrary, the CV dynamics in this setting shows no evident overshooting pattern but instead directly grows to the saturating values.

4. U(1)-Asymmetric Initial States with U(1) Non-Symmetric Hamiltonian. Next we investigate dynamics with U(1)-asymmetric initial states under H_1 where EA dynamics depends on both symmetry-breaking parameters, θ and γ. θ describes the symmetry breaking in the initial state while γ describes the symmetry breaking in the Hamiltonian. The interplay between these two parameters results in distinct behaviors in the EA dynamics. This is illustrated in the schematic figures with varying θ and γ in Figs. 2(c) and 2(d). The colors highlight the tendency of EA at early times. The blue regime indicates that $\Delta S_{L/4}(t)$ never exceeds its initial value for early times, while the red regime corresponds to the situations where EA can grow larger than its initial value at early times. It is clearly reflected in Fig. 2(a), the initial growth of EA at $\theta = 0.2\pi$ and $\gamma = 0.8$, 0.6 aligns with the red region. For a fixed γ, EA grows with weaker asymmetric effects (small θ) in the initial states or for a fixed θ, EA increases with stronger symmetry breaking effects (large $1-\gamma$) in the Hamiltonian. Consequently, the early-time behavior of EA serves as a witness to compare the symmetry-breaking strength hosted by the quantum state and the Hamiltonian.

Another key feature of the early-time dynamics is the emergence of QME, as shown in Fig. 2(a) for the symmetric case $\gamma = 1$. The origin of this QME lies in the relatively small ZZ term and gapless nature in the Hamiltonian.[42] QME persists for ferromagnetic (antiferromagnetic) states when $0.8 \leq \gamma \leq 1$ ($0.4 \leq \gamma \leq 1$). We also report relevant results for non-integrable Hamiltonian H_2 in the SM, and the results remain qualitatively consistent with those from the case of H_1, demonstrating the universal applicability of conclusions in this Letter for Hamiltonian evolutions.

Our simulation on the other symmetry-breaking measure, CV, reveals that QME can also emerge for CV with initial tilted ferromagnetic states, but only in cases of non-symmetric evolution. The reversed monotonicity of CV with respect to θ can persist even at late times. Table 1 summarizes the early- and late-time behavior of EA and CV for different initial states. The distinction shows the richness in characterizing symmetry breaking strength and patterns.

Table 1. The early- and late-time behavior of EA and CV under the evolution of H_1 or H_2 ($0.5 \leq \gamma \leq 1$). Crossing in EA (CV) means when the time-evolution curves of EA (CV) for states with larger θ intersect with those for smaller θ at early times. The right-up (right-down) arrow indicates that the late-time value is increasing (decreasing) with increasing tilted angle θ.

	Ferromagnetic	Domain wall	Antiferromagnetic
EA (early time)	Crossing for small $1-\gamma$	Crossing for small $1-\gamma$	Crossing for small $1-\gamma$
CV (early time)	Crossing for $\gamma \neq 1$	No crossing	No crossing
EA (late time)	↗	↗	↗
CV (late time)	↘	↗	↗

5. U(1)-Symmetric (Asymmetric) States with U(1) Non-Symmetric Random Circuit. A schematic diagram of the circuit architecture is shown in Fig. 3(a). The circuit under consideration consists of 16 qubits. We evaluate the EA at different P_{Haar}, using an antiferromagnetic initial state. We observe that EAs approach zero at late times, as illustrated in Fig. 3(b). This behavior can be understood in the context of quantum thermalization and information scrambling,[61–64] where the reduced density matrix of the subsystem is a fully mixed state for the random circuit cases, as long as the subsystem size does not exceed half of the total system. Additionally, for all probabilities chosen in Fig. 3(b), EAs reach their maximum after only a few layers of unitaries. The rate of symmetry restoration also depends on the initial state. In the SM, we find that symmetry restoration occurs more quickly for antiferromagnetic or domain wall states than for ferromagnetic states, due to the larger Hilbert space sector of the initial states in the former cases. In Fig. 3(c), we reveal that the peak of the circuit-averaged EA, $\mathbb{E}[\Delta S_{L/4}]_{\max}$ follows a power law with respect to P_{Haar} for small P_{Haar}.

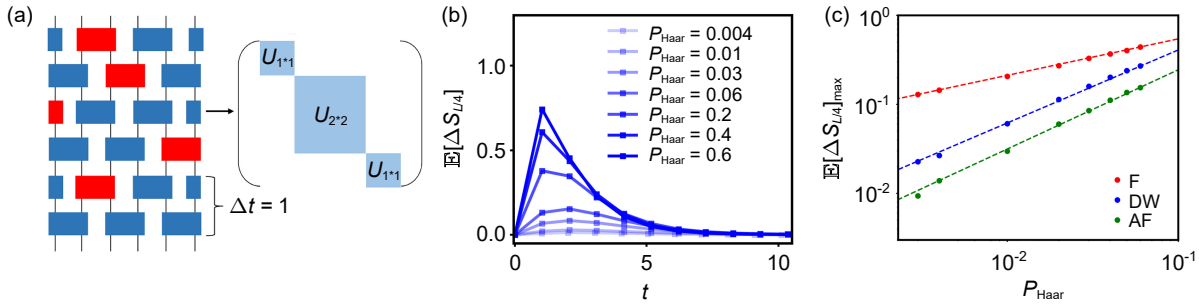

Fig. 3. (a) Schematic illustration of a non-symmetric random circuit with 6 qubits. Gates are arranged in the even-odd brick-wall pattern. The blue and red rectangles represent U(1)-symmetric and random Haar gates, respectively. The basis for the U(1)-symmetric gate is listed in the following order: $|00\rangle$, $|01\rangle$, $|10\rangle$ and $|11\rangle$. (b) The circuit-averaged EA, $\mathbb{E}[\Delta S_{L/4}]$, as a function of time with the antiferromagnetic initial state at different values of P_{Haar}. (c) The peak value, $\mathbb{E}[\Delta S_{L/4}]_{\max}$, as a function of P_{Haar}. All three curves follow a power law $y = ax^b$. F: Ferromagnetic state ($a = 1.4$, $b = 0.4$); DW: Domain wall state ($a = 2.7$, $b = 0.8$); AF: Antiferromagnetic state ($a = 1.9$, $b = 0.9$).

Next, we examine the dynamics from U(1)-asymmetric initial states, i.e., a tilted ferromagnetic state. We compute the EA for both U(1) symmetry with $\hat{Q}_a = \sum_{i\in a} \sigma_i^z$ and Z_2 symmetry with $\hat{Q}_a = \prod_{i\in a} \sigma_i^z$. As depicted in Fig. 4(a), for $P_{\text{Haar}} = 0$, we clearly notice the emergence of QME in U(1) case. Surprisingly, we also find that the QME appears in the Z_2 probe, which does not contradict previous study[25] suggesting the absence of QME in Z_2-symmetric circuits. Even though U(1)-symmetric gates are also Z_2 symmetric, there is no off-diagonal coupling between $|00\rangle$ and $|11\rangle$, leading to different thermalization rates between two Z_2 charge sectors ($Q_a = \pm 1$), and thus resulting in QME. As we replace a portion of U(1)-symmetric gates with random Haar gates, QME remains evident with a finite number of random Haar gates. However, when the circuit consists entirely of random Haar gates, all charge sectors thermalize at the same rate after circuit averaging, and QME disappears. In this case, the overshooting mechanism becomes apparent: EA curves for all initial states (parametrized by θ) converge to a

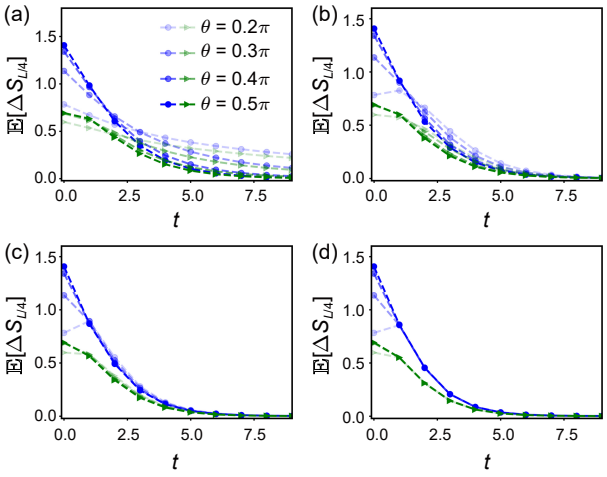

Fig. 4. The circuit-averaged EA, $\mathbb{E}[\Delta S_{L/4}]$, as a function of time for different values of P_{Haar}. Blue: U(1) EA. Green: Z_2 EA. Panels (a)–(d) correspond to different values of P_{Haar}. (a) $P_{\text{Haar}} = 0$, (b) $P_{\text{Haar}} = 0.3$, (c) $P_{\text{Haar}} = 0.7$, and (d) $P_{\text{Haar}} = 1$, respectively.

common finite value after a single gate layer, then decay toward zero at late times. Overshooting occurs when this transient value exceeds the initial EA of certain states—particularly symmetric initial states.

6. Conclusions and Discussions. In this Letter, we present a comprehensive study of subsystem symmetry breaking within two frameworks: a non-symmetric Hamiltonian evolution and a non-symmetric random circuit. Our simulation reveals that U(1) symmetry is always restored in the non-symmetric random circuit case, regardless of the initial states or the density of symmetry-breaking random Haar gates P_{Haar}. On the contrary, subsystem U(1) symmetry remains broken in the case of a U(1) non-symmetric Hamiltonian.

In addition to the late-time results, the early-time dynamics of EA shows a universal and surprising feature of overshooting. Specifically, the initial growth of EA can reach a peak significantly higher than its late-time steady value. This behavior is unexpected and is distinct from the growth of entanglement or CV, another measure of symmetry breaking, where the value increases monotonically to its saturating level without any evident overshooting. Furthermore, for asymmetric initial states evolved under non-symmetric Hamiltonians, the distinct and rich early-time dynamics of EA (increase versus decrease) allow for a direct comparison of the symmetry-breaking extent in both the state and the Hamiltonian.

There are several promising directions for further exploration. For instance, studying the dynamics of symmetry breaking in a non-unitary random circuit with mid-circuit measurements[65–81] could offer valuable insights. Additionally, examining the effect of symmetry breaking in Hamiltonians that avoid thermalization such as many-body localization systems[45,82–90] can provide a more unified picture of the understanding of symmetry-breaking dynamics.

Acknowledgement. HY acknowledges the support of the International Young Scientist Fellowship of the Institute of Physics, Chinese Academy of Sciences (Grant No. 202407). SXZ is supported by the Innovation Program for Quantum Science and Technology (Grant No. 2024ZD0301700) and the start-up grant at IOP-CAS. ZXL is supported by the Beijing Natural Science Foundation (Grant No. JR25007) and the National Natural Science Foundation of China (Grants No. 12347107 and 12474146).

References

[1] Bernstein J 1974 *Rev. Mod. Phys.* **46** 7
[2] Deutsch J M 1991 *Phys. Rev. A* **43** 2046
[3] Srednicki M 1994 *Phys. Rev. E* **50** 888
[4] D'Alessio L, Kafri Y, Polkovnikov A, and Rigol M 2016 *Adv. Phys.* **65** 239
[5] Rigol M, Dunjko V, and Olshanii M 2012 *Nature* **481** 224
[6] Deutsch J M 2018 *Rep. Prog. Phys.* **81** 082001
[7] Mpemba E B and Osborne D G 1969 *Phys. Educ.* **4** 172
[8] Lu Z and Raz O 2017 *Proc. Natl. Acad. Sci. U.S.A.* **114** 5083
[9] Lasanta A, Vega Reyes F, Prados A, and Santos A 2017 *Phys. Rev. Lett.* **119** 148001
[10] Kumar A and Bechhoefer J 2020 *Nature* **584** 64
[11] Klich I, Raz O, Hirschberg O, and Vucelja M 2019 *Phys. Rev. X* **9** 021060
[12] Teza G, Yaacoby R, and Raz O 2023 *Phys. Rev. Lett.* **131** 017101
[13] Bechhoefer J, Kumar A, and Chétrite R 2021 *Nat. Rev. Phys.* **3** 534
[14] Malhotra I and Löwen H 2024 *J. Chem. Phys.* **161** 164903
[15] Kumar A, Chétrite R, and Bechhoefer J 2022 *Proc. Natl. Acad. Sci. U.S.A.* **119** e2118484119
[16] Manikandan S K 2021 *Phys. Rev. Research* **3** 043108
[17] Chatterjee A K, Takada S, and Hayakawa H 2023 *Phys. Rev. Lett.* **131** 080402
[18] Aharony Shapira S, Shapira Y, Markov J, Teza G, Akerman N, Raz O, and Ozeri R 2024 *Phys. Rev. Lett.* **133** 010403
[19] Wang X and Wang J 2024 *Phys. Rev. Research* **6** 033330
[20] Nava A and Fabrizio M 2019 *Phys. Rev. B* **100** 125102
[21] Carollo F, Lasanta A, and Lesanovsky I 2021 *Phys. Rev. Lett.* **127** 060401
[22] Chatterjee A K, Takada S, and Hayakawa H 2024 *Phys. Rev. A* **110** 022213
[23] Ivander F, Anto-Sztrikacs N, and Segal D 2023 *Phys. Rev. E* **108** 014130
[24] Ares F, Murciano S, and Calabrese P 2023 *Nat. Commun.* **14** 2036
[25] Liu S, Zhang H K, Yin S, and Zhang S X 2024 *Phys. Rev. Lett.* **133** 140405
[26] Turkeshi X, Calabrese P, and De Luca A 2024 arXiv:2405.14514 [quant-ph]
[27] Fagotti M, Collura M, Essler F H, and Calabrese P 2014 *Phys. Rev. B* **89** 125101
[28] Essler F H L and Fagotti M 2016 *J. Stat. Mech.* **2016** 064002
[29] Doyon B 2020 *SciPost Phys. Lect. Notes* 18
[30] Fagotti M 2014 *J. Stat. Mech.* **2014** P03016
[31] Bertini B and Fagotti M 2015 *J. Stat. Mech.* **2015** P07012
[32] Vidmar L and Rigol M 2016 *J. Stat. Mech.* **2016** 064007
[33] Alba V, Bertini B, Fagotti M, Piroli L, and Ruggiero P 2021 *J. Stat. Mech.* **2021** 114004
[34] Calabrese P, Essler F H L, and Mussardo G 2016 *J. Stat. Mech* **2016** 064001
[35] Polkovnikov A, Sengupta K, Silva A, and Vengalatorre M 2011 *Rev. Mod. Phys.* **83** 863
[36] Bastianello A, Bertini B, Doyon B, and Vasseur R 2022 *J. Stat. Mech.* **2022** 014001
[37] Ares F, Murciano S, Vernier E, and Calabrese P 2023 *SciPost Phys.* **15** 089
[38] Klobas K, Rylands C, and Bertini B 2024 arXiv:2406.04296 [cond-mat.stat-mech]
[39] Rylands C, Klobas K, Ares F, Calabrese P, Murciano S, and Bertini B 2024 *Phys. Rev. Lett.* **133** 010401
[40] Yamashika S, Ares F, and Calabrese P 2024 *Phys. Rev. B* **110** 085126
[41] Khor B J J, Kürkçüoglu D M, Hobbs T J, Perdue G N, and Klich I 2024 *Quantum* **8** 1462
[42] Rylands C, Vernier E, and Calabrese P 2024 *J. Stat. Mech.* **2024** 123102
[43] Ares F, Murciano S, Piroli L, and Calabrese P 2024 *Phys. Rev. D* **110** L061901
[44] Murciano S, Ares F, Klich I, and Calabrese P 2024 *J. Stat. Mech.* **2024** 013103
[45] Liu S, Zhang H K, Yin S, Zhang S X, and Yao H 2024 arXiv:2408.07750 [cond-mat.dis-nn]
[46] Chang W X, Yin S, Zhang S X, and Li Z X 2024 arXiv:2409.06547 [cond-mat.str-el]
[47] Russotto A, Ares F, and Calabrese P 2024 arXiv:2411.13337 [hep-th]

[48] Joshi L K, Franke J, Rath A *et al.* 2024 *Phys. Rev. Lett.* **133** 010402
[49] Rossi L, Barbiero L, Budich J C, and Dolcini F 2023 *Phys. Rev. B* **108** 155420
[50] Fisher M P, Khemani V, Nahum A, and Vijay S 2023 *Annu. Rev. Condens. Matter Phys.* **14** 335
[51] Capizzi L and Vitale V 2024 *J. Phys. A: Math. Theor.* **57** 45LT01
[52] Chen M and Chen H H 2024 *Phys. Rev. D* **109** 065009
[53] Capizzi L and Mazzoni M 2023 *J. High Energ. Phys.* **2023** 144
[54] Ares F, Murciano S, Calabrese P, and Piroli L 2025 arXiv:2501.12459 [cond-mat.stat-mech]
[55] Lessa L A, Ma R, Zhang J H, Bi Z, Cheng M, and Wang C 2024 arXiv:2405.03639 [quant-ph]
[56] Sala P, Gopalakrishnan S, Oshikawa M, and You Y 2024 *Phys. Rev. B* **110** 155150
[57] Li Z, Zheng H, Wang Y, Jiang L, Liu Z W, and Liu J 2023 arXiv:2309.16556 [quant-ph]
[58] Hearth S N, Flynn M O, Chandran A, and Laumann C R 2023 arXiv:2306.01035 [cond-mat.stat-mech]
[59] Li Z, Zheng H, Liu J, Jiang L, and Liu Z W 2023 arXiv:2309.08155 [quant-ph]
[60] Zhang S X, Allcock J, Wan Z Q *et al.* 2023 *Quantum* **7** 912
[61] Chen Y Q, Liu S, and Zhang S X 2024 arXiv:2405.05076 [quant-ph]
[62] Hayden P and Preskill J 2007 *J. High Energ. Phys.* **2007** 120
[63] Sekino Y and Susskind L 2008 *J. High Energ. Phys.* **2008** 065
[64] Lashkari N, Stanford D, Hastings M, Osborne T, and Hayden P 2013 *JHEP* **2013** 022
[65] Hosur P, Qi X L, Roberts D A, and Yoshida B 2016 *JHEP* **2016** 004
[66] Skinner B, Ruhman J, and Nahum A 2019 *Phys. Rev. X* **9** 031009
[67] Choi S, Bao Y, Qi X L, and Altman E 2020 *Phys. Rev. Lett.* **125** 030505
[68] Li Y, Chen X, and Fisher M P 2019 *Phys. Rev. B* **100** 134306
[69] Jian S K, Liu C, Chen X, Swingle B, and Zhang P 2021 *Phys. Rev. Lett.* **127** 140601
[70] Minato T, Sugimoto K, Kuwahara T, and Saito K 2022 *Phys. Rev. Lett.* **128** 010603
[71] Dhar S and Dasgupta S 2016 *Phys. Rev. A* **93** 050103
[72] Vijay S 2020 arXiv:2005.03052 [quant-ph]
[73] Bao Y, Choi S, and Altman E 2020 *Phys. Rev. B* **101** 104301
[74] Gullans M J and Huse D A 2020 *Phys. Rev. X* **10** 041020
[75] Zabalo A, Gullans M J, Wilson J H, Gopalakrishnan S, Huse D A, and Pixley J 2020 *Phys. Rev. B* **101** 060301
[76] Ippoliti M, Gullans M J, Gopalakrishnan S, Huse D A, and Khemani V 2021 *Phys. Rev. X* **11** 011030
[77] Szyniszewski M, Romito A, and Schomerus H 2019 *Phys. Rev. B* **100** 064204
[78] Jian C M, You Y Z, Vasseur R, and Ludwig A W 2020 *Phys. Rev. B* **101** 104302
[79] Liu S, Li M R, Zhang S X, and Jian S K 2024 *Phys. Rev. Lett.* **132** 240402
[80] Liu S, Li M R, Zhang S X, Jian S K, and Yao H 2024 *Phys. Rev. B* **110** 064323
[81] Liu S, Li M R, Zhang S X, Jian S K, and Yao H 2023 *Phys. Rev. B* **107** L201113
[82] Alet F and Laflorencie N 2018 *Cr. Phys.* **19** 498
[83] Abanin D A, Altman E, Bloch I, and Serbyn M 2019 *Rev. Mod. Phys.* **91** 021001
[84] Pal A and Huse D A 2010 *Phys. Rev. B* **82** 174411
[85] Nandkishore R and Huse D A 2015 *Annu. Rev. Condens. Matter Phys.* **6** 15
[86] Imbrie J Z, Ros V, and Scardicchio A 2017 *Annalen der Physik* **529** 1600278
[87] Altman E and Vosk R 2015 *Annu. Rev. Condens. Matter Phys.* **6** 383
[88] Huse D A, Nandkishore R, and Oganesyan V 2014 *Phys. Rev. B* **90** 174202
[89] Lukin A, Rispoli M, Schittko R, Tai M E, Kaufman A M, Choi S, Khemani V, Léonard J, and Greiner M 2019 *Science* **364** 256
[90] Morningstar A, Colmenarez L, Khemani V, Luitz D J, and Huse D A 2022 *Phys. Rev. B* **105** 174205